Volume 2
№ 2, 2020

ISSN: 2706-977X

MATERIAL AND MECHANICAL ENGINEERING TECHNOLOGY

Material and Mechanical Engineering Technology. MMET.KZ

Editorial board

Content

Investigation of the parameters of an aerodynamic device causing a vortex air flow

Dyussembina A.G., Duisenbayeva M.S, Madi P.Sh., Nesina Y.G., Abiljanova F.B.
Karaganda Technical University, Karaganda, Kazakhstan

Abstract: The article is devoted to studying the parameters of an aerodynamic installation that causes a vortex air stream. In the study of the velocity field of the vortex wind flow created by the designed installation, the following dependence was constructed: a graph of the velocity in the flow propagated from the screw air, depending on the distance from the screw at y = + 37 cm, y = 0, y = -37 cm With the help of an aerodynamic installation creating a whirlwind wind stream, the velocities in the flow distributed from the propeller at each distance are determined. Distance from the air and the most airflow y=+37 cm, y=0, y=-37 cm the connection schedule for available speeds is specified. $\frac{x}{d}$ - the ratio of the distance to the diameter of the propeller, $\frac{U}{U_{max}}$ - the ratio of the speed spread from the propeller to the maximum speed.

Key words: air, propeller, wind, aerodynamic installation, speed, airflow.

1. Introduction

A number of measures are currently being taken to optimize the use of wind energy and to develop wind turbines that are non-traditional sources of energy. On behalf of President N.A. Nazarbayev, Kazakhstan has developed a strategy for the efficient use of renewable energy and resources for sustainable development by 2024. This program was developed as part of the Development Program and Development Project of the Ministry of Energy and Mineral Resources of Kazakhstan "Kazakhstan - the beginning of the development of the wind energy market".

An example of an aerodynamic device generating an uneven velocity wind flow is shown in Figure 1 below. The aerodynamic unit consists of a solid wood double-bladed air rifle, a DKM-1UHL4 type engine, supports and baffle [1].

Fig. 1. - An example of an aerodynamic device that generates a wind flow

The blades of an air rifle are elliptical in shape and rotate around a circle. The screw rotates the propeller clockwise. Screw length 40 cm and weight 80.8 g.

The main parameters of the wind flow generated using a model of an aerodynamic device. The main parameters of the propeller model and engine are shown in Table 1.

Table 1

The main parameters of the propeller model	
Made material	solid wood
Number of blades	2
Length	40 cm
Weight	80.8 g
Screw diameter	30 cm
Number of revolutions	1200 rpm
Top speed	10 m / s
The main parameters of the engine	
Type	DKM-1WXL4
Voltage	220
Power	1,5 kW
Frequency	50 Hz

2. Results and discussion

Aerodynamic installations capable of creating a vortex wind flow were determined at speeds from 3 m to 15 m, y = + 37 cm, y = 0, y = -37 cm in the air flow [2-4].

Change in air velocity from bolt to y = + 37 cm, y = 0, y = -37 cm. The current flows from the propeller are shown in Table 2.

Table 2

x, m	Current flows from the propeller		
	y = + 37 cm speed	axial speed (y = 0)	y = -37 cm speed
1	12	0	12
3	9,9	4,6	9,9
6	7,5	7,1	7,4
9	5,6	5,8	5,6
12	3,2	3,4	3,1
15	1,3	1,5	1,3

Figure 2 shows a graph of the change in speed at a given point during the experiment, when the speed at which the air flow was y = + 37 cm, y = 0, y = -37 cm

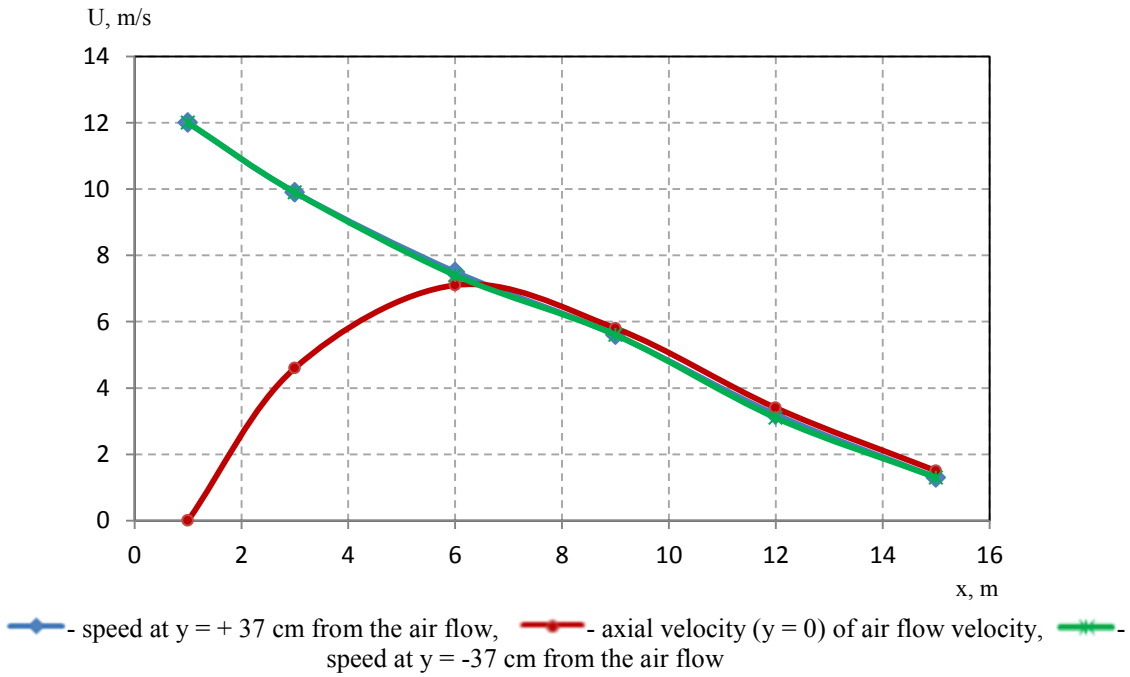

Fig. 2. - The graph of the air velocity from yoke to y = + 37 cm, y = 0, y = -37 cm

An aerodynamic installation generating a whirlwind in outer space created an air velocity from speeds of 1.3 m/s to 12 m/s. In the experiment, speeds from 1 to 15 meters were detected. As can be seen from the graph showing the dependence U = f (x) in Fig. 2, the air flow velocities at y = + 37 cm, y = -37 cm decrease with increasing distance, and the axial velocity in the air flow is zero at the first 1 m. Then, when the spindle lengthened to 6 m, the axis velocity was 7.1 m / s. After the axis reached a maximum speed of 7.1 m/s, the speed decreased with increasing distance.

Figure 3 shows a graph of the speeds between the distance and the air speed at y = + 37 cm, y = 0, y = -37 cm. Where x/d is the ratio of the distance to the diameter of the air rifle, U/Umax is the ratio of the speed transmitted by the air rifle to the maximum speed. The diameter of the air rifle is 1.5 m, and the maximum air velocity through the spindle is 12 m/s.

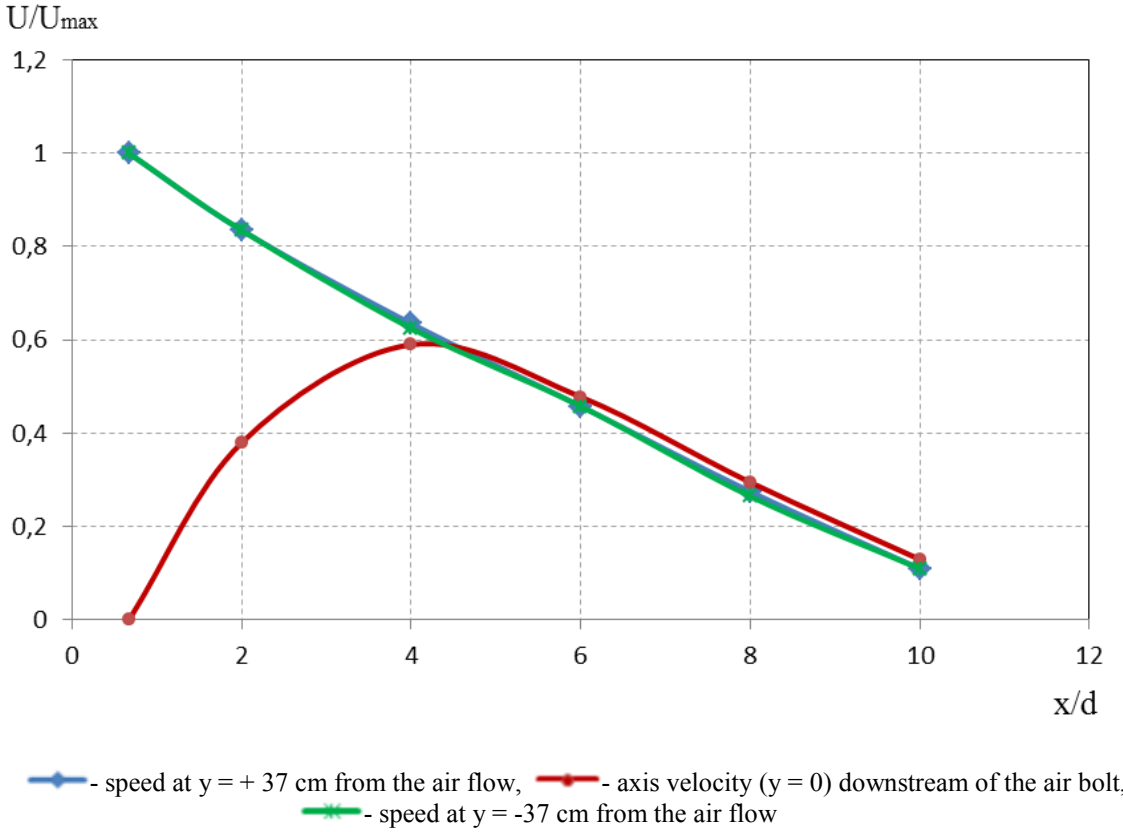

Fig. 3 - The relationship between the distances and air flow velocities at a speed of y = + 37 cm, y = 0, y = -37 cm

As can be seen from the relative dependence of the speed and speed of the airspace on the diameter of 1.5 m and 30 cm, as you can see, the greater the distance, the lower the rotation speed of the air rifle [5-7].

Experience with changing the number of rotations in an aerodynamic installation that causes wind flow in open space. During the experiment, a control panel was used that regulates the amount of rotation to change the amount of rotation of the propeller. At different distances, from 1 m to 15 m, the velocity in the flow distributed from the propeller is determined, with a change in the number of rotation from the control panel. When changing the number of rotation of the propeller, the speed change is given in the presence of $U = f(x) \rightarrow y = +37$ cm, $U = f(x) \rightarrow y = 0$, $U = f(x) \rightarrow y = -37$ cm, depending on the distance from the propeller.

The change in speed depending on the distance between the speeds in $U = f(x) \rightarrow y = +37$ cm, $U = f(x) \rightarrow y = 0$, $U = f(x) \rightarrow y = -37$ cm from the spread flow when changing the number of rotation of the propeller.

The parameters speed depending on the rotation of the propeller (Table 3).

Table 3

n, rpm	in the stream spread from the propeller																	
	speed at y= + 37 cm						the axial (y=0) speed						speed at y= -37 cm					
	x, 1 м	x, 3м	x, 6 м	x, 9 м	x, 12м	x, 15 м	x, 1 м	x , 3м	x, 6 м	x, 9 м	x, 12м	x, 15 м	x, 1 м	x, 3м	x, 6 м	x, 9 м	x, 12м	x, 15 м
120	4,1	3,3	2,3	1,4	0,6	0	0	1,3	2,1	1,6	0,8	0,2	4,1	3,3	2,4	1,4	0,7	0
360	5,6	4,5	3,7	2,8	0,9	0,3	0	2	3,5	2,7	1,5	0,5	5,6	4,5	3,7	2,8	0,9	0,3
510	6,8	5,7	4,4	3	1,7	0,6	0	2,7	4	3,4	2,1	0,9	6,8	5,7	4,3	3	1,8	0,6
830	9,7	7,1	5,9	4,2	2,6	0,9	0	3,4	5,9	4,6	2,9	1,1	9,6	7,1	5,9	4,2	2,6	0,9
1000	12	9,9	7,5	5,6	3,2	1,3	0	4,6	7,1	5,8	3,4	1,5	12	9,9	7,5	5,3	3,1	1,3

Figure 4 shows a graph of changes in the speed depending on the distance from the screw in the presence of $U = f(x) \rightarrow y = +37$ in the widespread air flow with the amount of rotation of the propeller 120 rpm, 510 rpm, 1000 rpm

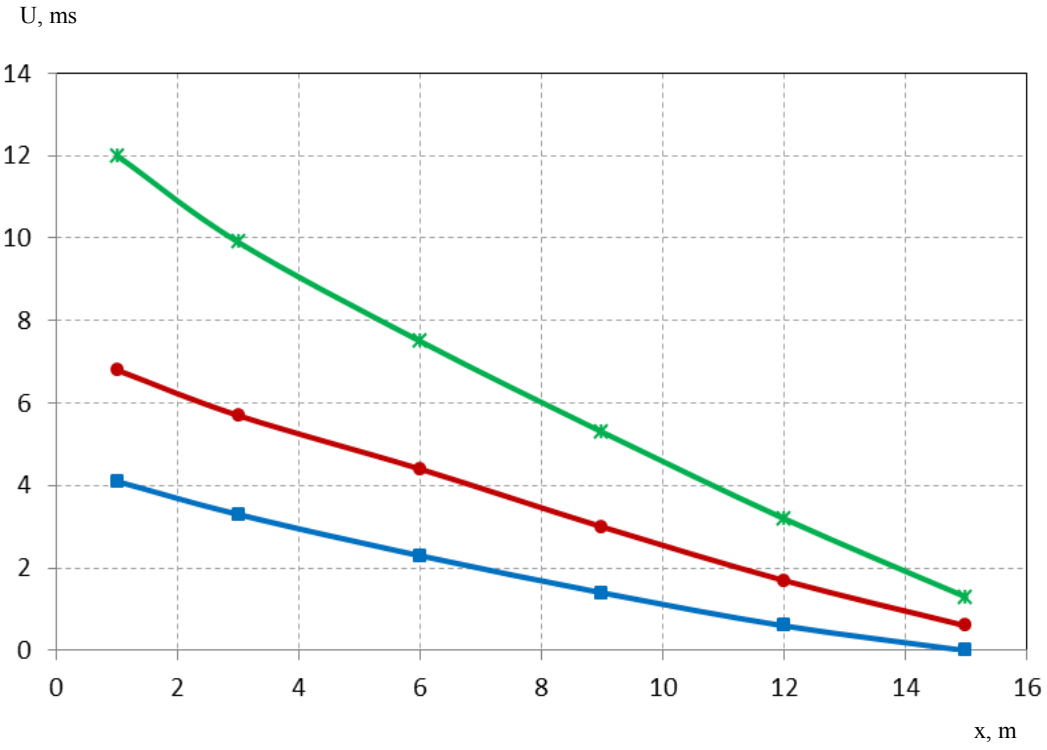

- the speed at rotation of the propeller y = +37 cm in the spread flow from the propeller at the amount of rotation of the propeller 120 rpm, - the speed of rotation of the air screw at a pressure y = + 37 cm from the air screw at the amount of rotation of the air screw 510 rpm, - the speed of rotation of the air screw at a pressure y = + 37 cm from the air screw at the amount of rotation of the air screw 1000 rpm

Fig. 4. - Graph of speed changes in the presence of $U = f(x) \rightarrow y = +37$ cm in the widespread flow from the propeller at the amount of rotation of the propeller 120 rpm, 510 rpm, 1000 rpm depending on the distance from the screw

As can be seen from the graph in figure 4, it can be seen that the flow rate from the propeller decreases as it elongates from the propeller. In addition, as the number of rotations of the propeller increases, the speeds in the flow propagated from the propeller increase.

In open space, an experiment was conducted with changing the number of rotation in an aerodynamic installation that causes wind flow. The aerodynamic unit consists of two bladed wooden propellers with a length of 1.5 m, engines and supports with a power of 7.5 kW. The main element of the installation is an air screw. The weight of the screw is 25 kg. The experience for determining the speed of the propeller was developed in open space.

3. Conclusions

Considering the energy efficient use of renewable energy requires a lot of work, a lot of research. A good knowledge of this energy will make a significant contribution to the country's economy [8-10].

From the experiments obtained to study the aerodynamics of an aerodynamic installation generating wind in outer space, the following conclusions can be drawn:

Using an aerodynamic device that generates a vortex wind flow in open space, speeds were obtained at each distance from 3 m to 15 m, y = + 37 cm, y = 0, y = -37 cm and a dependency graph was constructed. , From a graph showing the dependence U = f (x), it was found that the air flow from the air rifle decreases with increasing distance at y = + 37 cm, y = -37 cm, and that the axial velocity in the air flow from the air rifle becomes zero in the first 1 m.

References

[1] Duisenbayeva M.S., Nesina Y.G., Dyussembina A.G., Madi P.Sh., Abiljanova F.B., Kenzhebek A.S. Study of the aerodynamic parameters of the installation, generating wind flow in open space. Published under licence by IOP Publishing Ltd. Journal of Physics: Conf.Series, Volume1327, Number 1. DOI:10.1088/1742-6596/1327/1/012007

[2] Sibikin Yu.D., Sibikin M.Yu. 2010 Unconventional and renewable energy sources (M: Zhnorus)

[3] Bychkov N.M. 2005 Wind turbine with Magnus effect. Characteristics of the rotating cylinder Thermophysics and Aeromechanics 1 59-175

[4] Suslov A.D., Ivanov S. V., Murashkin A.V., Chizhikov Yu. V. Vortex apparatuses: - M. Ed. "Mashinostroenie", 1985. -256 p.

[5] Kuzmin G. I. Air screws: Textbook for aircraftt technicians. - M, 1937. - 141 p.

[6] Kusaiynov K , Tanasheva N. K , Turgunov M. M , Kalikova A and Dysembaeva A 2013 The effect of porosity on the aerodynamic characteristics of a rotating cylinder Eurasian Physical Technical Journal 2 (20) 26-32

[7] Kussaiynov K, Tanasheva N, Stoev M, Nussupbekov B, Dysembina A, Alkenova A, and Kussaiynova A 2015 The research of aerodynamic characteristics of a rotating cylinder with variable cross section Proceedings of the Sixth International Scientific Conference-FMNS2015 66-70

[8] Mihnenkov L.V. 2002 Wind power plant of planetary type Scientific Bulletin of MSTU GA, series Operation of air transport and repair of aircraft. Flight safety 49 110-13

[9] Yurchenko A.V., Zotov L.G., Mekhtiev A.D., Yugai V.V and Tatkeeva G.G. 2015 Power supply of autonomous systems using solar modules IOP Conference Series: Materials Science and Engineering 81(1) 012112

[10] Mihnenkov L.V., Markotenko G.A. 2001 Patent 2169858 of the Russian Federation. Planetary wind power unit NDTS

Scientific and engineering bases for development of mobile overpasses

Kadyrov A. A. [1], Ganyukov A.A.[1], Balabekova K.G. [2], Zhunusbekova Zh.Zh. [1], Suleev B.D.[1]
[1]The Karaganda Technical University, Karaganda, Kazakhstan
[2] The Eurasian National University named after L.N.Gumilev, Nur-Sultan, Kazakhstan

Abstract: A new type of transport equipment has been developed that is mobile overpass (mobile bridge crossing). The proposed mobile overpasses are used to eliminate traffic blocks on urban highways, as well as during the repair of urban utilities. They allow continuous movement of motor vehicles through various obstacles: traffic jams, trenches formed because of underground repair works or emergency situations (earthquakes, floods, etc.).

Key words: mobile overpasses, modular overpasses, temporary bridges, traffic jams, elimination of traffic blocks, calculation for strength and stability.

1. Introduction

In conditions of intensive urban road traffic there are traffic blocks and jams due to various reasons: car accidents, rush hours, repair works on roads, urban utilities, etc. In many large cities there is a task to solve the problems of traffic jams during natural traffic and during repair of urban infrastructure. For big cities, this is a great transport problem. As it is known traffic jams and blocks on city highways worsen the transport logistics of the city, ecology, cause economic damage to entrepreneurs, the budget of the city, etc.

To solve the above-mentioned problems, we offer several structures of mobile overpasses: road and communal. They are assembly-disassembled mobile bridge crossings, which are installed on top of road lanes where traffic block has occurred or on those sections where underground repair of city utilities under roads takes place, which facilitates transport driving on the emergency or repair section and, accordingly, eliminates car traffic jams and eliminates the need to bypass repair sections of roads (Figure 1, Figure 2) [1, 2].

Fig.1 - Mobile road overpass

The use of overpasses offered by us significantly improves transport logistics in the city during traffic jams or repair works on communal networks: reduces the formation of car traffic jams, releases forced bypass of repair sections, reduces inconvenience for drivers of cars and residents of districts of the city, through which forced bypass of transport would take place.

Such mobile crossings can be used not only for the elimination of traffic blocks and underground repair works in urban conditions, but also in emergency situations caused by flood, earthquake, resulting in the destruction of various infrastructure such as roads, bridges, crossings, etc.

a) Transport position

b) Superstructure above trench

b) Operational position

Fig.2 - Mobile Communal Overpass

A distinctive feature of the proposed overpasses is their mobility that is driving on their own chassis by means of an automobile trailer or on a truck. Quick assembly and disassembly at the site of its installation due to application of unified assembly-disassembling modules and methods of their attachment to each other and on the ground base. This ensures fast delivery to the necessary sections with auto-transport, repair sections of communal underground networks or to sections with damaged infrastructure caused by various emergencies.

The analysis of the state of this topic in Kazakhstan, CIS and abroad showed almost complete absence of such mobile bridge structures to eliminate car traffic jams, urban repair needs and emergency conditions.

Certain elements of the subject have been partially developed in the military bridge structure - skewed trawls, automobile bridge laying, etc. This issue has not been developed in civil transport construction and requires comprehensive study and creation of scientific foundations for the creation and design of mobile overpasses for different conditions of their operation. Thus, mobile overpasses have no analogues in the world and are, in fact, a new type of transport vehicles.

2. Types of overpasses

The road mobile overpass is designed to eliminate traffic blocks on urban highways. It is assembled from six separate metal modules, each of which is a combination of the roadway roadway (structurally orthotropic plate) and a bearing spatial frame in the form of four posts connected by longitudinal and transverse bearing beams (Figure 3). All modules are equipped with their own wheel chassis for transportation and retractable supports. The modules are transported to the intersection by a tractor, assembled and interconnected by grippers into a single structure. At the same time retractable supports rest on road base.

Spatial stiffness from horizontal forces along the crossing (braking forces) and horizontal forces across the crossing (wind load) is perceived by the communication system (Figure 3).

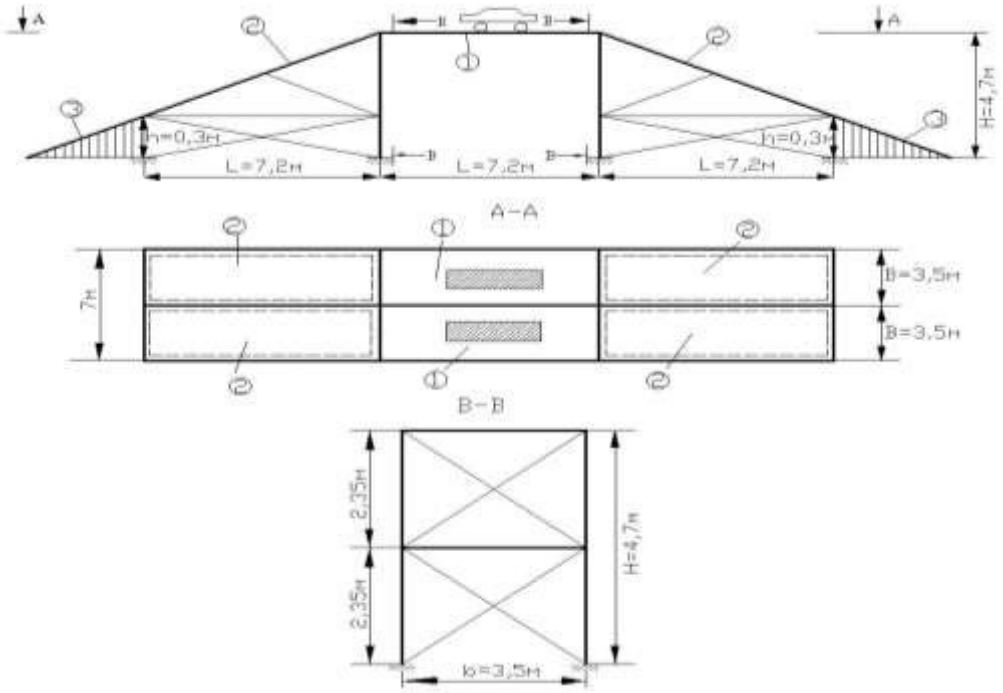

1 – two orthogonal modules; 2 – four inclined modules; 3 – access ramp

Fig.3 – Scheme of road mobile overpass

The road overpass should meet the overall structure conditions of the roadway: the height of passage under it is not more than 4.5m, the width of the transport lane in one direction is not less than 3.5m (for the conditions of the Republic of Kazakhstan). (Figure 1, Figure 3). The construction load on the road is up to 4 t/m^2, which corresponds to the passage of motor ehicles with the weight up to 3.5 t. The material of all elements is structural steel C235 and C245.

Mobile road overpass has two main modules: inclined (Figure 4,a) and horizontal (Figure 4,b).

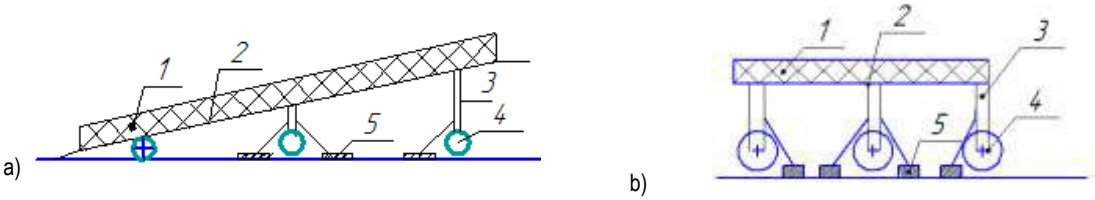

1 – barrier; 2 – plate; 3 – support; 4 – wheels; 5 - support and mechanism of its lifting

Fig.4 - Main modules of the mobile overpass

The patent [3] is obtained for the proposed design of the mobile overpass.

The assembled structure allows driving of part of the motor vehicles over the perpendicular road and its use at various crossroads, as its dimensions are controlled by the number of modules (Figure 1). The mobile two-lane bridge crossing is delivered by cars to the problem site, and assembled within 15 to 20 minutes. Installation of the structure is performed by lifting of wheels and extension of outriggers (Figure 5)

Modules are connected due to deployment of extensible sections at the highest point and lowering of additional sections at the lower point. The presence of the overpass on the road will be informed by a dynamic information board. Vehicles turn left should make turn at the next crossroad. After the block is eliminated, the overpass is disassembled into several modules and towed to its location. The operation of assembling and disassembling of the overpass is automated and does not take much time due to specially designed mechanisms of fixing parts of the overpass, both between themselves and with the roadway.

The overpass may also be single-lane. In single-lane form, the overpass is assembled from three metal modules: one orthogonal and two inclined modules. The use of a mobile overpass reduces the cost of building huge overpasses and junctions, and does not require a large area of road.

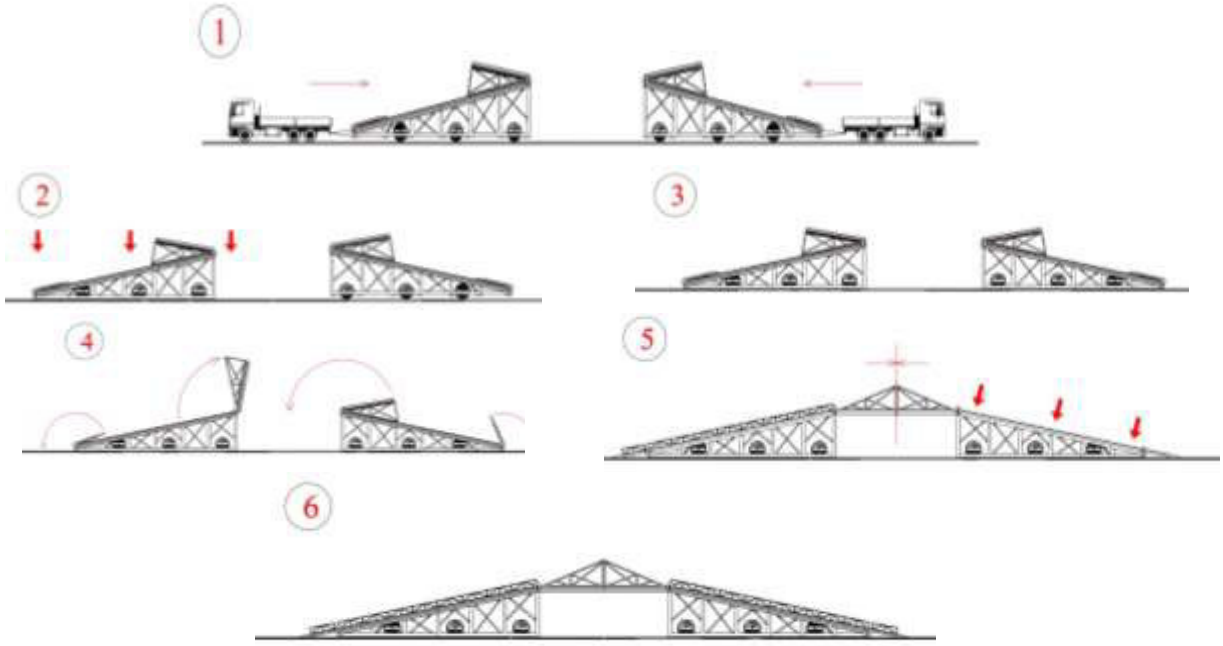

Fig.5 - Road mobile overpass assembly

In order to create a reliable overpass design, it is necessary to obtain different dependencies between the load of mobile transport and the operation of all units, which allow to develop a technique for calculation of the design of the mobile road overpass. In addition, during operation, the overpass is supported by supports on the asphalt surface of the road, which can result in the destruction of the asphalt surface.

On the basis of the above, the work study and calculations of the road overpass are determined by:

- establishment of the optimal length of one module of the mobile overpass taking into account the width of the roadway;
- calculation of bearing structures of mobile overpass frames;
- numerical experiment on the operation of the orthotropic plate of the roadway;
- experimental-analytic modeling of mobile overpass support.

Therefore, it is necessary to test the operation of the overpass support system. The requirement for operation of the overpass support is that the asphalt-concrete surface under the support should work in the elastic deformation zone so plastic changes do not occur, i.e., the surface of the asphalt concrete surface should not be disturbed. The aim of the study is to establish the parameters of the support and the value of the load on the supports at which the asphalt concrete coating operates in the zone of elastic deformations.

The disadvantage of the road overpass for elimination of traffic jams is the impossibility of its use through open repair tranches of communal networks, as its supports rest on the middle of the roadway (Figure 1). In such cases, a mobile overpass used during the repair of utilities such as heat, water, cable, etc. can be used to eliminate the above-mentioned disadvantage (Figure 2). Usually, urban utilities are located under roads. During their repair there is a break of repair trenches on the site of roads, which causes their closure for a long time and the need to organize various long-term uncomfortable bypass. Under these conditions, instead of forced bypass routes of repair trenches, we propose to organize direct crossings through them - mobile communal overpasses. Such an overpass is installed through repair trenches of communal networks and allows non-stop traffic flows in the area of repair sections of roads for the whole period of underground repair (Figure 2). The use of a communal overpass significantly improves the transport situation in the city during repair works.

The municipal mobile overpass is a single-span bridge crossing, which combines the bearing structure of the roadway and the wheeled running gear, which allows to transport it to the place of operation on the trailer by a tractor. Such integration of the bridge structure with its own chassis mechanism, both in the communal overpass and in the road overpass, determines a new type of transport equipment - mobile overpasses (Figure 1, 2).

Figure 2, a shows a schematic 3D model of a mobile utility overpass in transport position (transport mode): the overpass moves to its place of operation by a tractor on a rigid coupling on its own running gear to the place of operation or storage. After the overpass is delivered, it is stretched over the trench along the guide metal shelves installed over the trench (Figure 2,b). Figure 2.1 shows the overpass in the operating position. After the overpass is transversally slided over the trench, it is transferred to the operational position (bridge mode) by lifting the driving wheels and lowering the load-bearing structure with the help of mounting jacks onto concrete supports, which are entrance ramps on the overpass roadway (Figure 2, c). The overpass installed in such a way makes direct crossing of repair trenches of communal networks by transport flows, which eliminates the need to bypass repair areas and

form traffic jams and blocks. The transfer of overpass from "bridge mode" to "transport mode" is performed accordingly in reverse order.

The essence of the proposed structures is that they are both a vehicle and a bridge (overpass), which is a new type of transport equipment - mobile overpasses [4, 5].

From the structural point of view, the mobile overpass consists of a metal bearing structure of the roadway, which is put on a two-axle wheel chassis - running gear (Figure 6, positions I and V).

The load-bearing structure of the mobile overpass is intended for passage through it of motor vehicles and it is a single-span structure without components (Figure 6, position I). The design provides the transfer of transport through trenches up to 8m wide. The width of the roadway of the overpass bearing structure is 2,5m, with the design load on the roadway up to 3 t/m^2. Such load ensures the passage of vehicles with loaded weight up to 2,5t, which corresponds to motor low-loaded vehicles in urban conditions of operation [5].

a) Side view

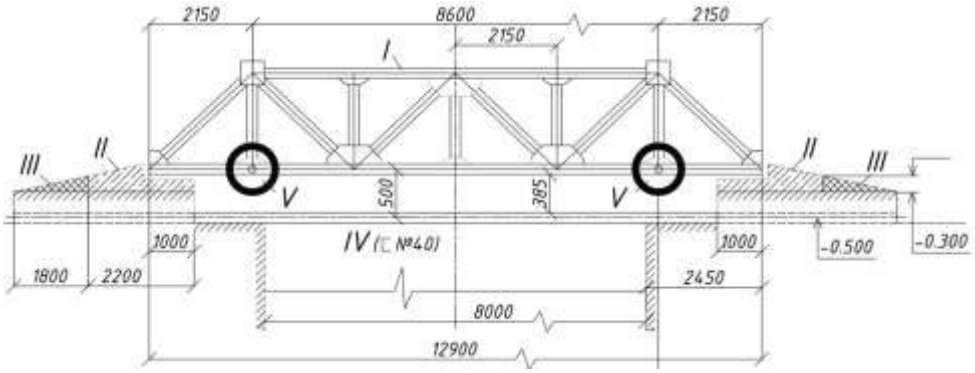

b) Top view

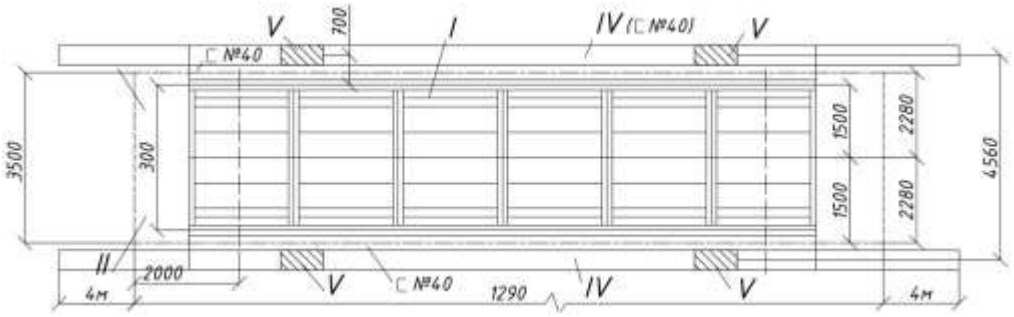

I - bearing structure of overpass roadway; II - reinforced-concrete overpass supports; III - ground entry ramps; IV - metal guide rails; V - running gear with driving wheels in raised position.

Fig.6 - Structural scheme of the mobile overpass

The bearing structure is designed from two bridge trusses with "bottom driving" of the roadway, which is a system of longitudinal and transverse beams covered with corrugated metal flooring, 20 mm thick (Figure 6, a, b, position I). The span of load-bearing structure is 12,9m with width along axes of trusses 3 m (Figure 6, b). Roadway trusses and beams are designed from I-beam section. The material of all elements is structural steel C235 and C245. The weight of overpass bearing structure is 9.5t.

The overpass is equipped with its own running gear and is delivered to the installation site by means of a tractor on a trailer. Running gear of overpass consists of 2 axles: front turning and rear non-turning, which are rigidly connected to transverse beams of carrying structure of roadway along lower outer belts of trusses (Figure 6, position V). Front rotary axle provides "way-handling" of overpass during its transportation. After delivery, it is installed by means of sliding over trenches with the help of guide rails, which are bridged over the trench. After the sliding, the overpass structure is lowered onto reinforced concrete supports. For this purpose running gear of overpass is equipped with specially designed mechanisms of wheel lifting and turning.

Additional inventory equipment of the overpass is guide metal skids (Figure 6, position IV) and reinforced concrete supports (Figure 6, position II). The skid guides are used for sliding the overpass over the open trench span during the preparation of its transfer from "transport mode" to "bridge mode." The skids that are at least 13m long, (Figure 6, position IV) consist of a reinforced channel.

Reinforced concrete supports of mobile overpass are reinforced concrete foundations with shaped cross-piece (Figure 6, a, b, position II). The foundations are simultaneously entry ramps for transport to the overpass. The

foundations of supports prevent bearing structure of overpass from longitudinal and transverse displacement by means of their penetration into ground with depth up to 30 cm. Supports and guide rails may be transported on the overpass itself during its transportation to the place of operation or storage.

The combined overpass structure, combining the roadway support structure and the running gear (Figure 6, positions I and V), experiences different traffic and operational loads. Therefore, an important issue in the study of overpass operation is the determination of loads during its transportation and operational position. When transporting the overpass, the loads, vibrations and forces that occur in the overpass design are different from those that occur when driving along the overpass when it is operating in the operational position. And therefore, the frequencies of oscillations and the forces by which we must determine the strength of the structures are in different frequency ranges. Thus, we have a task in which it is necessary to determine the design parameters of the overpass, which operates in different ranges of loads and vibrations.

In addition, these loads and vibrations are transmitted to the ground through the concrete supports of the overpass (Figure 6, position II). The effect of these loads leads to the accumulation of deformation energy in the ground base, which can lead to the collapse of trench sides and an emergency situation during the operation of the overpass. This determines the development of a technique on the optimal arrangement of overpass supports, to prevent collapse of trench sides taking into account the real properties of the ground base on the basis of a non-linear model of ground deformation.

On the basis of the above, the study and calculations of the overpass are determined by the fact that the elements of the overpass structure operate in different load ranges and form two joint systems: "bearing structure - running gear"; “overpass supports - ground base”. This requires a comprehensive study:

- operation of load-bearing structure and running gear, their calculation and design;
- operation of the system "overpass support - ground base" to prevent collapse of trench sides and optimal arrangement of overpass supports taking into account the properties of the ground base on the basis of a non-linear ground model, which increases the accuracy of calculations.

3. Main results

Our research group has developed scientific and theoretical bases for calculation and design of mobile overpasses of various types, including design solutions for creation of all its parts and nodes.

Volume-planning and design solutions have been developed for creation of unified modules of mobile overpasses, providing the required carrying capacity of its roadway for passage of type and quantity of rolling stock determined by standards of automobile bridge structure. In this case, the shapes and dimensions of the structural cross sections are also pre-selected for further calculations.

Calculations of orthotropic plates of the roadway of bridge crossings were carried out by various numerical methods, such as the method of finite elements, finite differences, etc.

The stress-deformed state of spatial frames of overpasses is investigated on the basis of calculations of force state by analytical displacement method with formation of common matrices, taking into account parametric variability of geometric and rigidity characteristics of bearing elements of spatial frames. This allows the automatic calculation of similar frames for bridge crossings of different design and purpose. Here the final selection of the cross sections of the structural structures of the spatial frame is carried out on the basis of the standard conditions of strength, rigidity and stability taking into account the specific requirements for the structures of the automobile bridge structure [6.7].

The operation of bearing flat statically-indeterminated trusses of overpasses by analytical method of forces has been investigated. Here, the influence of the rigidity characteristics of the truss rods is studied, the changes of which can have a significant result on the power and tension state of the truss as a whole.

A mathematical model of operation of the support of the road overpass with variable mass has been developed.

Interaction of support devices of overpass with natural ground base was investigated and analysis of stressed state of ground massif in zone of trench sides based on nonlinear model of Drucker-Prager ground deformation was developed. On this basis, practical bases of calculation for strength and stability of the corresponding volume of ground mass under load from pressure of overpass support devices have been developed. The method of optimal arrangement of supports for prevention of board collapse during overpass operation has been developed [8].

Various types of overpasses supports, chassis structures, mechanisms for modules connection to which corresponding patents and certificates of intellectual property have been obtained have been developed.

In order to create an efficient design solution of mobile overpasses, methods of optimization calculations have been developed on the basis of mathematical theory of optimization in order to minimize metal consumption of structures to reduce their cost.

Bearing structures of all types of overpasses are made of reinforced steel grades. Preliminary selection of cross sections of bearing elements of tracks of all types is carried out on the basis of conditions of strength, rigidity, stability with sufficient reserve taking into account possible overloads and dynamic effect of movement on the roadway of rolling stock. The value of bridge loadings is accepted according to the Euro-norms.

Machine-building drawings of overpass prototype design, methods of overpass installation, recommendations for its operation and assessment of economic effect have been developed.

4. Conclusion

The studies made it possible to propose a new type of transport equipment - mobile overpasses, which allow to eliminate road congestion on roads, during car traffic jams and repair of urban communal networks.

For the first time, the general calculation technique has been developed, allowing for the simultaneous calculation of the overpass as a bridge structure and as a vehicle for various loads.

The developed general technique of calculation and design of mobile overpasses used in repair of urban communal networks can be recommended to scientific and engineering workers of transport and machine-building industry, as well as design and research institutes. The initial data on the specific use of the results are the results of the research and experimental works carried out.

The theoretical bases of calculations developed and described above allow to design overpasses of various types on a practical basis, starting with the development of their structural solution, selection of cross sections of bearing structures according to conditions of their strength, rigidity and stability taking into account various loads, both static and dynamic, arising from the movement of rolling stock along the roadway. Using optimal design methods, you can create cost-effective and reliable overpass designs.

The theoretical and applied developments described herein provide reliable and cost-effective solutions for designing and constructing practical mobile overpasses for various purposes.

References

[1] Kadyrov A.S., Balabekova K.G., Ganyukov A.A., Akhmediyev S.K. The constructive solution and calculation of elements of the unified module of the mobile bridge overcrossing // Transport problems. – Poland: The Silesian University of Technology, 2017. - Volume 12. - P. 59 -71.

[2] Ganyukov A.A., Kadyrov A.S., Balabekova K.G., Imanov M. Research and calculation of constuctive elements of mobile overpass// Current Science online submission and processing – India, 2019 – Volume 9. P. p.1544-1550 .

[3] Patent for Utility Model RK № 3219. Semi-overpass/A.S. Kadyrov, K.G. Balabekova, A.A. Ganyukov; publ. 09.10.2019. – P. 3.

[4] Kadyrov A., Ganyukov A. Balabekova K. Development of Constructions of Mobile Road Overpasses. The 2017 International Conference on Mechanical, Aeronautical and Automotive Engineering «MATEC Web of Conferences (ICMAA 2017)», Malacca, Malaysia, February 25-27, 2017, Volume 108 (2017)

[5] Ganyukov A.A., Georgiadi I.V. Calculation and design of construction elements of mobile overpass.//Works of the University. - Karaganda: KarSTU, 2018, № 4 (73). - P. 104-111

[6] Ganyukov A.S., Kadyrov A.S., Balabekova K.G., Kurmasheva B.K. Tests and calculations of structural element of temporary bridges. Roads and Bridges. – Poland: Road and bridge research institute, 2018. – Volume 17. – p.215-226.

[7] A.Kadyrov, A.Ganyukov S.Amanbayev, K.Balabekova, B.Kurmasheva. Solving Traffic Congestion Problems and Definition Stress-Strain State of Curvilinear Overpass Module Sector-Ring Slab // International Journal of Engineering and Advanced Technology. – Damkheda, Bhopal (Madhya Pradesh), India, 2020, Volume 9, Issue 3. – P. 44-48

[8] Aliyev S.B., Kadyrov A.S., Ganyukov A.A. Study of strength and stability of trench boards of communal networks from the impact of the load of the modular overpass.//Fundamental research. - Russian Federation: Academy of Natural Science, 2017, № 5. – P. 15-20

Determining the temperature field of circular saws

Bakirov Zh.B., Bakirov M. Zh., Mikhailov V.F.
Karaganda Technical University, Karaganda, Kazakhstan

Abstract: The problem of determining the temperature field in circular saws with diamond segments along the outer contour is solved. The thermal conductivity equation for such disks is derived and boundary conditions are formulated. The specific heat flow and temperature field are represented as a Fourier series expansion along a circumferential coordinate. For each harmonic, the exact solution of the thermal conductivity equation is found in the form of a combination of modified Bessel functions. When solving the problem, the disk cooling method is taken into account. As a result of the solution and reasonable simplification, an axisymmetric temperature field is obtained, which changes exponentially along the radius of the disk. The results can be used to evaluate the stability of the flat shape of the balance of circular saws and the stability of diamond segments.

Keywords*:* circular saw, stone processing, thermal conductivity equation, temperature field, Nusselt criterion, Bessel functions.

1. Introduction

An important task in mechanical engineering is to create metal-cutting tools for processing high-strength materials. Analysis of existing cutting methods shows that the solution to this problem often involves the creation and use of high-performance machines and mechanisms with disk actuators equipped with diamond segments, which are used for sawing metal workpieces or destruction of various materials. During operation, circular saws are subjected to cutting and feeding forces, inertia forces, and temperature fields. All these loads act in the plane of the cutting disc and can cause a loss of stability of the disc saws.

A large amount of theoretical and experimental studies in the use of saws with diamond segments in the stone and mining industry performed in institutes ISI Almaz, CISI Podzemmash (Moscow), IAS of Ukraine (Kyiv), RISS (Yerevan), Institute of Nerud (Tolyatti), KarPTI, KNIUI (Karaganda) [1-3]. Similar studies were conducted in the United States, Germany, England, the Czech Republic, Slovakia and Poland. At the same time, issues related to the study of the influence of physical and mechanical properties of rocks and cutting modes on the energy and force indicators of destruction, wear and temperature conditions of the tool were considered. Despite a large amount of research, not enough attention is paid to determining the temperature field of disk saws. It was set in various ways, most often in the form of a power function over the radius, the coefficients of which were determined experimentally.

Most journal articles on this topic are devoted to determining the temperature field of brake discs [4-6]. The closest approach to this problem is the article [7], where the influence of the temperature field of a disk cutter on the destruction of rocks is studied. In these works, the finite element method [5-7] or the grid method [4] is used to solve heat conduction problems. In [8], an experimental-analytical method is proposed for determining the temperature field, when measured temperature values are initiated at individual points on the experimental setup, which are modelled using the green function. The thermal conductivity problem is solved by the method of integral transformations using the measured boundary values of the temperature field.

This article offers an analytical method for determining the temperature field in disk saws.

2. Methods and solution of basic relations

To derive the thermal conductivity equation, select an element with dimensions dr and $rd\theta$ from the disk. Then the amount of heat entering the element during *dt* can be determined by the formula [4]:

$$Q_1 = h\lambda\nabla^2 T r\, dr\, d\theta\, dt,$$

where h is a plate thickness;

λ is a thermal conductivity;

$\nabla^2 = \frac{\partial^2}{r^2\,\partial\,\theta^2} + \frac{\partial}{r\,\partial r} + \frac{\partial^2}{\partial r^2}$ is a harmonic operator in polar coordinates.

Heat transfer from the surface of the element due to convective heat exchange is equal to:

$$Q_2 = 2\alpha(T - T_c) r dr d\theta dt,$$

where T_c is an ambient temperature;

α is an average heat transfer coefficient.

By rotating the disk, the selected element moves along the circumferential coordinate. During *dt* its temperature changes by a value of

$$dT = \frac{\partial T}{\partial \theta} \cdot \frac{\partial \theta}{\partial t} \partial t = \frac{\partial T}{\partial \theta} \omega dt,$$

where ω is an angular speed of disk rotation.

In this case, the amount of heat changes by a value of

$$Q_3 = C\rho h \, dr \, dt \, dT d\theta,$$

where C, ρ are specific heat capacity and density of the material.

The heat balance equation has the form

$$Q_1 = Q_2 + Q_3.$$

Dividing both parts of the equation by $r \cdot dr d\theta dt$ we get

$$h\lambda \nabla^2 T = 2\alpha(T - T_c) + C\rho h\omega \, \partial T / \partial \theta.$$

Moving to the dimensionless radius $x = r/R$ we have

$$\nabla^2 T - m^2 T - p \frac{\partial T}{\partial \theta} = 0, \quad (1)$$

where T is the disk temperature exceeds the ambient temperature;

$m^2 = 2\alpha R^2 / h\lambda$ is a Bio criterion;

$p = VR/a$ is a Peclet criterion;

$a = \lambda / C\rho$ is a thermal diffusivity of the material;

V is a circumferential speed on the outer contour of the disk of radius R.

The circular saw consists of a steel body and an annular abrasive layer with an outer radius of R_H. Then the boundary conditions for the thermal conductivity equation have the form:

$$\begin{aligned} &\lambda_c \, \partial T_1 / R \, \partial x + \alpha_H T_1 = q, \quad \text{if } x = \beta_H = R_H / R; \\ &\lambda_c \, \partial T_1 / \partial x = \lambda \, \partial T / \partial x, \quad T_1 = T \text{ if } x = 1; \frac{\partial T}{\partial x} = 0 \quad \text{if } x = \beta, \end{aligned} \quad (2)$$

where q is a specific heat flow;

λ_c is a coefficient of thermal conductivity of segments;

β is a dimensionless internal radius of the disk.

In the boundary conditions (2), heat transfer with the coefficient α_H from the cylindrical surface of the abrasive layer is taken into account. 1st index refer to the abrasive layer.

The average heat transfer coefficient is calculated using the Nusselt criterion [3]:

$$\alpha = N_u \lambda_{cp} / R, \quad (3)$$

where λ_{cp} is a thermal conductivity of the environment.

When cooling circular saws by air flow, the N_u criterion can be determined by the formula

$$N_u = 0.015 R_e^{0.8} - 100(\rho_{max}/R)^2, \quad (4)$$

where $R_e = VR/\nu_a$ is a Reynolds criterion;

ν_a is a kinematic air viscosity;

$\rho_{max} = 500(\nu_a/\omega)^{1/2}$ is the maximum radius of the laminar air flow zone.

When cooling with a liquid, it can be assumed that a turbulent flow occurs at [9]:

$$R_e = V_0 R/\nu_0 \geq 5 \cdot 10^5.$$

The Nusselt criterion is calculated using the formulas [3, 9]: for laminar flow

$$N_u = 0.8\sqrt{R_e}\,; \tag{5}$$

for turbulent flow $N_u = 0.043 R_e^{0.8}$.

The specific heat flow on the outer contour of the abrasive layer is decomposed into a Fourier series:

$$q = q_0 \sum_{n=0}^{\infty} (\ell_n \cos n\theta + g_n \sin n\theta) = q_0 \sum_{n=-\infty}^{\infty} C_n \exp(in\theta),$$

where q_0 is a characteristic value of heat flow.

The specific heat flow can be found from the ratio:

$$Q = \int_S q dS,$$

where S is the surface area of the heat flow;

Q is the amount of heat entering the disk per unit of time.

The value Q can be determined by the formula:

$$Q = 3600 N_p K_d / j \quad \text{(kcal/h)},$$

where N_p is the cutting power, kW;

K_d is a coefficient that takes into account the proportion of heat entering the disk;

j=4.187 is the thermal equivalent of mechanical energy.

Based on the representation of the heat flow and boundary conditions (2), we look for a solution (1) in the form:

$$T = \sum_{n=-\infty}^{\infty} T_n \exp(in\theta).$$

Then equation (1) for each term of the decomposition takes the form:

$$\left[\frac{d^2}{dx^2} + \frac{d}{xdx} - \left(m^2 + inp + \frac{n^2}{x^2}\right) T_n\right] = 0.$$

The solution to this equation has the form:

$$T_n = A_n I_n(kx) + B_n K_n(kx) \tag{6}$$

where I_n, K_n are modified Bessel functions of 1st and 2nd types;

- $k = (m^2 + inp)^{1/2}$.

The boundary conditions (2) can now be represented as

$$\begin{aligned} &x = \beta_H: \quad dT_{n_1}/dx + nT_{n_1} = \bar{q} C_n; \\ &x = 1: \quad \lambda\, dT_{n_1}/dx = \lambda dT_n/dx, T_{n_1} = T_n; \\ &x = \beta: \quad dT_n/dx = 0, \end{aligned} \tag{7}$$

where

$\bar{q} = q_0 R/\lambda_c$,

$n_H = \alpha_H R/\lambda_c$.

Substituting (6) in (7), we define constant integrations for the saw body, which are calculated using the following algorithm:

$$C_p = K_n(k_1)[k_1 I'_n(\beta_н k_1) + n_н I_n(\beta_н k_1)] - I_n(k_1)[k_1 K'_n(\beta_н k_1) + n_н K_n(\beta_н k_1)];$$

$$A_p = D_p I_n(k) - \frac{k\lambda}{k_1\lambda_c} C_p I'_n(k) - \frac{I'_n(\beta k)}{K'_n(\beta k)}\left[D_p K_n(k) - \frac{k\lambda}{k_1\lambda_c} C_p K'_n(k)\right];$$

$$A_n = -\frac{\bar{q}C_n}{k_1 A_p}; B_n = \frac{\bar{q}C_n}{k_1 A_p} \cdot \frac{I'_n(\beta k)}{K'_n(\beta k)}.$$

The A_p coefficient is determined from the expression for C_p by replacing $K_n(k_1)$, $I_n(k_1)$ with $K_n'(k_1)$, $I_n'(k_1)$, respectively. To simplify the obtained relations, we note that usually $\beta_H = 1{,}017 \ldots 1{,}02$, $\beta = 0{,}1 \ldots 0{,}3$;

$$k = (m^2 + inp)^{1/2} = [(\sqrt{n^2p^2 + m^4} + m^2)^{1/2} + i(\sqrt{n^2p^2 + m^4} - m^2)^{1/2}]/\sqrt{2}.$$

Since m^2 and m_c^2 are of order $10^2 \ldots 10^4$, p and p_1 are of order $10^5 \ldots 10^7$, then $np \gg m^2$, so $k \approx \lambda_n(1+i)$, where $\lambda_n = (np/2)^{1/2}$.

It follows that the Bessel functions when defining integration constants can be decomposed into a series for large argument values. Then, neglecting the higher-order terms of smallness, we get

$$T_n = -\frac{\bar{q}C_{\text{n}} \exp\left(-k(1-x)\right)}{k_1\sqrt{x}\left(D_p - C_{\text{p}}\frac{k\lambda}{k_1\lambda_c}\right)}. \tag{8}$$

To obtain a valid expression for the temperature field, we write it in the form of trigonometric Fourier series:

$$T = T_0 + \sum_{n=1}^{\infty}(T_{cn}\cos n\theta + T_{sn}\sin n\theta), \tag{9}$$

where $T_{cn} = T_n + T_{-n}$, $T_{sn} = i(T_n - T_{-n})$, $T_{-n} = -\bar{q}\frac{C_{-n}\exp(-k(1-x))}{\bar{k}_1\sqrt{x}\left(\bar{D}_p - \bar{C}_p\lambda\bar{k}/\lambda_c\bar{k}_1\right)}$.

In the last expression, symbols with a dash on top mean complex-conjugate numbers. After a sequence of mathematical transformations, we get

$$T_{sn} = \frac{2\bar{q}\sqrt{2\beta_H}\exp(-\gamma_n)}{\sqrt{np_1 x}}(K \cdot \cos\gamma_n - L \cdot \sin\gamma_n), \tag{10}$$

where

- $K = [(1 + n_H/\lambda_{n1})l_n - g_n]/E$;
- $L = [l_n + (1 + n_H/\lambda_{n1})g_n]/E$;
- $E = (1 + \sqrt{a_c/a} \cdot \lambda h/\lambda_c b_c)[1 + (1 + n_H/\lambda_{n1})^2]$;
- $\gamma_n = \lambda_n(1-x) + \chi_n$;
- $\chi_n = \lambda_{n1}(\beta_H - 1)$;
- l_n, g_n are the coefficients of decomposition of the specific heat flow into the Fourier trigonometric series.

The component T_{sn} is defined by the expression (10) replacing K by L and L by $(-K)$.

The axisymmetric component of the temperature field T_0 is found from (10), assuming $C_n = l_0$, $k_1 = m_c$, $k = m$, $C_p = [\text{ch}\chi_0 + (n_H/m_1)\text{sh}\chi_0]/\sqrt{\beta_H}$, where $\chi_0 = m_c(\beta_H - 1)$.

The coefficient D_0 is defined by the same expression by replacing ch with $(-\text{sh})$ and sh with $(-\text{ch})$. After elementary transformations we get

$$T_0 = \bar{q}l_0\sqrt{\beta_H/x}\exp[-m(1-x)]/m_c D_0, \tag{11}$$

where $D_0 = \left(n_H/m_c + {m\lambda}/{m_c\lambda_c}\right)\mathrm{ch}\chi_0 + \left(1 + {m\lambda n_H}/{m_c^2\lambda_c}\right)\mathrm{sh}\chi_0$.

The change in the temperature field is estimated by the circumferential coordinate on the outer contour of the saw body. In this case, expression (10) can be rewritten as

$$T = \frac{\bar{q}l_0\sqrt{\beta_H}}{m_c D_0}\left\{1 + \sum_{n=1}^{\infty}\frac{\sqrt{8}m_c D_0}{\sqrt{np_1}\exp(\chi_n)}[K\cos(n\theta - \chi_0) + L\sin(n\theta - \chi_0)]/l_0\right\}.$$

Analysis of this expression shows that under the sign of the sum is an exponentially decreasing series, each member of which is negligible in comparison with the unit at significant rotation speeds. Therefore for disk saws, the temperature field can be considered axisymmetric and changing along the radius of the disk according to the law

$$T = T_H\exp[-m(1-x)]/\sqrt{x}. \quad (12)$$

The temperature of the outer contour of the cutting disc body, taking into account the decrease in temperature due to the presence of intersegment slots, can be written as:

$$T_H = \bar{q}\sqrt{\beta_H}C_c/m_c D_0, \quad (13)$$

where C_c is the coefficient of discontinuity of the outer surface of the disk due to intersegment grooves.

For an axisymmetric temperature field, you can easily find the temperature in the cutting zone. To do this, in expressions (7), replace T_0 with the expression (11)

$$\left.\begin{aligned} A_0 I'_0(m_c x) + B_0 K'_0(m_c x) &= (\bar{q}/m_c D_0)\sqrt{2\pi m\beta_H}\exp(-m)I'_0(mx) \\ A_0 I_0(m_c x) + B_0 K_0(m_c x) &= (\bar{q}/m_c D_0)\sqrt{2\pi m\beta_H}\exp(-m)I_0(mx) \end{aligned}\right\} x = 1.$$

From here, after simplification and transformation, we get

$$A_0 = \bar{q}\sqrt{2\pi\beta_H/m_c}\exp(-m_c)/D_0, \qquad B_0 = \bar{q}\sqrt{\beta_H/2\pi m_c}\exp(m_c)/2mD_0.$$

Substituting them in (6), assuming $x = \beta_H$, we get the temperature in the cutting zone

$$T_p = \bar{q}\exp(\chi_0)[1 + \exp(-2\chi_0)/4m]/m_c D_0. \quad (14)$$

With sufficient cooling, the second term in parentheses can be ignored.

3. Results

To perform specific calculations, you need to know the coefficient of heat transfer to the disk. It depends on the thermal properties of the rock and segment, on the cutting modes, on the granularity and concentration of diamonds in the segment. The formula for determining the coefficient of heat transfer to the product during grinding has the form [2]:

$$\alpha_m = \left[1.25\frac{\lambda_c}{\lambda_m}\sqrt{\frac{a_m}{h_{cp}V}} + 1\right]^{-1}, \quad (15)$$

where a_m is the thermal diffusivity of the product;

λ_c, λ_m is a thermal conductivity of the segment and product;

h_{cp} is the average chip thickness cut by a diamond grain, determined by the formula [1].

$$h_{cp} = 0.8r_a\lambda_p(\varphi_k - 0.16\sin 2\varphi_k - 0.012\sin 4\varphi_k)/\varphi_k,$$

where r_a is a radius of the diamond grains;

λ_p is a coefficient of cutting modes;

φ_k is an angle of contact of the disk with the product.

The coefficient of cutting modes is determined by the formula:

$$\lambda = 14.5\left(\frac{V_n}{VC_cK_0}\right)^{\frac{1}{2}},$$

where V_n is a feed rate;

K_0 is a volume concentration of diamond in segments as a percentage.

The coefficient of heat transfer to the disk is now equal to $K_d = 1 - \alpha_m$.

As follows from the formula (12), the temperature field of the disk is determined by two parameters: m and T_n. When the design parameters of the saw and the thermal properties of the materials (disk, segment, product) are known, the temperature of the outer contour of the disk and the temperature in the cutting zone can be expressed in terms of a specific heat flow. Here is the procedure for calculating these parameters:

- depending on the properties of the cooling medium, we use the formula (3) to determine the average heat transfer coefficient;
- defining the Bio criteria for the disk and for segments (m and m_c);
- determine the coefficients n_H, χ_0 and using the formula (11) determine the coefficient D_0;
- using the formula (13), we determine the temperature of the outer contour of the disk through the specific heat flow;
- using the formula (14), we determine the temperature in the cutting zone.

Figure 1 shows a graph of the dependence of the temperature field parameters on the speed of the coolant when cutting granite. These values are accepted for calculations:

λ =38.5 kcal/m h °C, λ_c=72 kcal/m h°C;

for granite [10]:

λ_m = 3,5 kcal/m h°C, C_m = 0,74 kcal/kg ºC, ρ_m = 2720 kg /m^3;

for an aqueous solution [9]:

λ_o = 0,52 kcal/m h°C, η =10 kg/m s, $\nu_o = \eta/\rho = 10^{-6}$ m^2 /s. , $R_e = 4 \cdot 10^5$;

for the saw: R = 0,4 m, h = 4 mm, β_H = 1,015.

The sharp increase in the Bio criterion at V_0 =1,25 m/s is explained by the transition of the flow from laminar to turbulent.

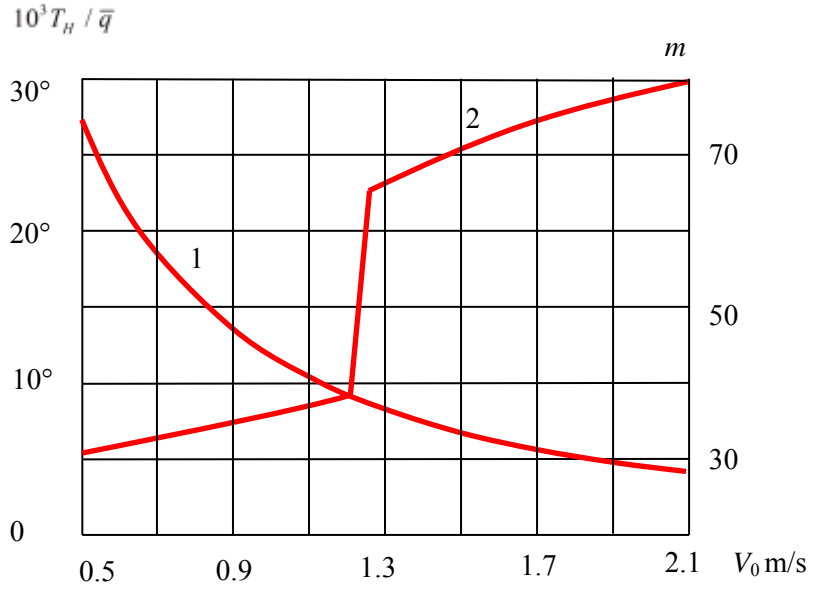

Fig 1 - Graph of the dependence of the temperature field parameters of the cutting disc on the speed of the coolant: curve 1 is the relative temperature $T_н/\overline{q}$; curve 2 is the Bio criterion m

When specific cutting modes and power are known, the temperatures in the circular saw can be determined explicitly. To do this, the heat transfer coefficient to the product and then to the disk is determined using the formula (15). Next is the specific heat flow:

$$\bar{q} = \frac{3600 K_d N_p}{2\pi j b_c \lambda_c \beta_H}.$$

To verify the results obtained, calculations were performed to determine the temperature field in saw disks by the finite element method using the ANSYS program [11]. Qualitative comparison of the results indicates that the obtained ratios are acceptable for practical calculations.

4. Conclusion

Based on the results of the research work, the following conclusions can be drawn:

1) the dependence of the temperature field parameters in disk saws on the cutting modes and thermal properties of materials: disk, segment, product and coolant is obtained;

2) it is found that for fast-rotating disks, the temperature field is axisymmetric and exponentially changing in radius.

The results obtained allow us to:

3) investigate the thermal stability of circular saws;

4) find a critical combination of operating parameters (cutting force, rotation speed, temperature field) from the stability condition of the plane form of equilibrium;

5) adjust the temperature in the cutting area from the tool life condition by selecting the coolant parameters.

References

[1] Diamond tool for destruction of strong rocks / A. F. Kichigin, S. N. Ignatov, Yu. I. Klimov, V. D. Yarema-Moscow: Nedra, 1980. -159 p.

[2] Cherkashin Yu. A., Nasybullin A. G. Diamond tools in stone processing. - Tashkent: Mehnat, 1986. - 159 p.

[3] Stakhiev Yu. M. Stability and vibrations of round circular saws. – M.: Forest industry, 1977. -284 p.

[4] Zhang, S., Zhang, J. Modeling and Analysis on Fluid-solid-thermal Physical Field Coupling of Ventilated Disc Brake. JixieGongchengXuebao/Journal of Mechanical Engineering. 2019. 55(8). - P. 154–164. DOI:10.3901/JME.2019.08.154.

[5] Zhou, S., Sun, C., Zhao, X., Qin, Z., Zhao, F. Simulation and Analysis of 3D Transient Temperature Field and Stress Field of Cast Steel Brake Disc of Intercity Trains. TiedaoXuebao/Journal of the China Railway Society. 2017. 39(8). Pp. 33–38. DOI:10.3969/j.issn.1001-8360.2017.08.005.

[6] Wen, H., Yang, F., Lv, W.Q., Chen, Y.X., Wang, Q.W. Finite Element Analysis of the Temperature Field of an Emergency Brake and Study of Its Thermal Properties. Strength of Materials. 2015. 47(1). - P. 136–142. DOI:10.1007/s11223-015-9639-x.

[7] An, Y., Li, M., Chen, S., Hu, Y., Zhang, A., Zhai, Y. Dynamic simulation and thermal analysis of rock breaking force on disc cutter of tunnel boring machine. Proceedings - 2019 4th International Conference on Mechanical, Control and Computer Engineering, ICMCCE 2019. - P. 1015–1020. DOI:10.1109/ICMCCE48743.2019.00227.

[8] Kulinchenko, G., Mozok, E. The study of thermal field of an object represented in the basis of Green functions.Eastern-European Journal of Enterprise Technologies. 2016. 5(5–83). Pp. 4–11. DOI:10.15587/1729-4061.2016.79570.

[9] Lykov A.V. Heat and mass transfer. – M.: Energiya, 1971. -560 p.

[10] Distribution and correlation of indicators of physical properties of rocks: Reference guide / M. M. Protodyakonov, R. I. Teder, E. I. Ilnitskaya, etc. - M.: Nedra, 1981. -192 p.

[11] Sherov K.T., Sikhimbayev M.R., Sherov A.K., Donenbayev B.S., Musayev, M.M. Mathematical modeling of thermofrictional milling process using ANSYS WB Software // Journal of Theoretical and Applied Mechanics, Sofia, Vol. 47, N. 2, 2017. - P.24-33. DOI:10.1515/JTAM-2017-0008.

Development of calculation methods for diesel locomotives of industrial transport

Rozhkov A. B., Balabayev O.T., Nartov M.A.
Karaganda technical university, Karaganda, Kazakhstan

Abstract. This article presents the results of studies carried out in the field of optimizing the driving of industrial diesel locomotive and developing the updated method of traction calculations. The main difference between industrial railway transport is the unevenness of the track profile (alternating steep slopes and platforms) over one stretch when driving long-line and heavy-weight freight trains. In extractive industries, such unevenness can be caused by general subsidence of the surface from production in mines. In conditions of uneven path profile, the main method of fuel economy is the use of kinetic energy of the entire composition, that is, it is required to increase the speed of the entire composition at a certain moment (before the start of lifting). In order to determine the appropriate slope resistance for each composition (wagon or locomotive) in the composition, it is necessary to determine the coordinates of each crew (its center) at a particular time. The authors also proposed a design scheme for the train, taking into account the resistance to the movement of each rail crew. Some of the results of the study were issued in the form of an application for copyright object, then a patent for utility model was obtained.

Keywords: railway transport, energy saving, industrial diesel locomotive, traction calculations, movement resistance, track profile, industrial transport.

1. Introduction

It is widely known that in many industries, rail transport, as a technological means for in-time supply of the production process with raw materials, has no alternatives in the form of vehicles or conveyors. However, in this mode of industrial transport is considered auxiliary undeservedly. If the "main" railway transport is the "railway industry," that is, a separate branch of the economy with a specific outcome product in the form of ton-kilometers of transported cargo and passenger turnover, then the contribution of industrial railway transport to the outcome products of metallurgical, mining enterprise or object of the thermal power complex is reduced to the result of one of many technological operations. At the same time, the operation of diesel locomotives at industrial enterprises has its own features, both obvious ones that are increased weight of trains and small radii of curves, and non-obvious ones that are high speeds of reaching the automatic (hyperbolic) traction characteristic, and even specific types of work in conditions of high temperatures and gas content of the foundry [1, 2]. However, at present time there is a significant technical lag in industrial rail transport from the magistral railways. For example, if in the countries of the European Union and the USA the production of specialized industrial diesel locomotives has been ongoing since the 50s of the last century, then only magistral or shunting diesel locomotives are still produced in the CIS. Naturally, there are no radical changes in the methods of traction calculations for diesel locomotives of industrial transport. Traction calculations for diesel locomotives at industrial enterprises are made according to the TCR method, with the only difference that personal computers and standard tools (MS Excel) or specialized programs (“Iskra TCR”, “Era”, “Vektrum”, etc.) are used for calculations [3].

In conditions of general tendency towards electrification of railway lines, diesel traction remains the main one in industrial railway transport. Electrified lines provide great savings, due to the low cost of electricity (compared to liquid fuel), but the need and capital intensity of building the entire electrification infrastructure make such savings possible only in the long term. Breaking the contact network on the railway line inevitably leads to expensive downtime in the entire technological process, and in this regard the autonomy of diesel locomotives leads to their widespread use. The characteristic exception is the use of electric locomotives and traction units in quarries. In this case, the need to create the expensive contact network on the "temporary" railway line with significant rises in slopes is dictated by the requirements of labor protection and the harmful effects of the ICE exhaust gases of the locomotive. Thus, due to the wide use of diesel traction in industrial railway transport, the development of energy-optimal methods of traction calculations for industrial transport, taking into account its specificity, is a relevant subject research [4, 5].

2. Results and discussion

The minimum fuel consumption by a diesel locomotive (in the absence of steep slopes) is achieved at a constant speed, that is, at an extreme $v=const$. This is because in the expression of resistance to movement there are terms that increase (linearly and quadratically) with an increase in speed. Therefore, any deviation from $v = const$ leads to an increase in the work required to overcome the resistance forces [6]. However, the main difference between industrial railway transport is precisely the unevenness of the track profile (alternating steep slopes and sites) over one stretch when driving long-line and heavy-weight freight trains. In extractive industries, such

unevenness can be caused by a general subsidence of the surface from production in mines. In conditions of uneven path profile, the generally accepted method of fuel economy is the use of kinetic energy of the whole composition, that is, it is required to increase the speed of the whole composition at a certain moment (before the start of lifting). However, it is not possible to solve the problem of accurate determining this time point for a particular lift using the method of the Traction Calculation Rules for Train Work (hereinafter - TCR). This is due to the fact that in the TCR the entire train composition is taken as a material point having mass, speed, acceleration, but without taking into account the total length of the cars and the locomotive.

The equation of movement of the train is the following:

$$F(\dot{s}, u) = (m_l + m_w \cdot n)\ddot{s} + W_{mov}(\dot{s}) + W_{sl.}(s), \quad (1)$$

where F is the traction force required for the train movement and it is a function of the speed $\dot{s}$(speed as a first derivative of the path *s*) and the position of the driver controller *u*;

m_l - locomotive mass;

m_w – mass of one wagon (the train is considered uniform, that is, consisting only of loaded or empty wagons) ;

n – number of cars in the train;

$\ddot{s}$ – acceleration expressed through the path as the second derivative;

$W_{mov.}$– force of resistance to movement, which is a function of the speed $\dot{s}$;

$W_{sl.}$– resistance force from the elements of the path profile, which is a function of the path s passed;

$W_{eng.}$ - is determined according to the procedure from TCR:

$$W_{eng.} = a + \dot{s} \cdot b + c \cdot \dot{s}^2, \quad (2)$$

where a, b, c - empirical coefficients.

The force of resistance to movement from the elements of the profile of the track W_{sl}, which is a function of the passed path *s*, and in the traditional TCR method is the sum of the resistance to movement of the locomotive and all wagons, while it is believed that the entire train (locomotive and all wagons) is on one element of the profile (slope, rise or site).

The force of resistance from the elements of the profile of the track W_{sl}, according to the design scheme of the train proposed by the authors, "flexible inextensible thread of articulated elements of the same mass" is equal to the sum of the forces of resistance to movement from the slope of the locomotive and all wagons, taking into account which element of the profile each rail crew is located [8, 9].

In order to determine the appropriate slope resistance for each crew (wagon or locomotive) in the composition, it is necessary to determine the coordinates of each crew (its center) at a particular time [10].

Moreover, the initial data are: n - the number of cars in the train; l_w - conditional length of the wagon; $l_{l\_}$ is the conditional length of the locomotive, the characteristic of the stretch (the available number of sections with corresponding slope values). Figure 1 shows the design layout of the train on the railway track.

We find the coordinate of the z-th wagon by the formula:

$$S_z = S - \frac{l_L}{2} - l_w \cdot z. \quad (3)$$

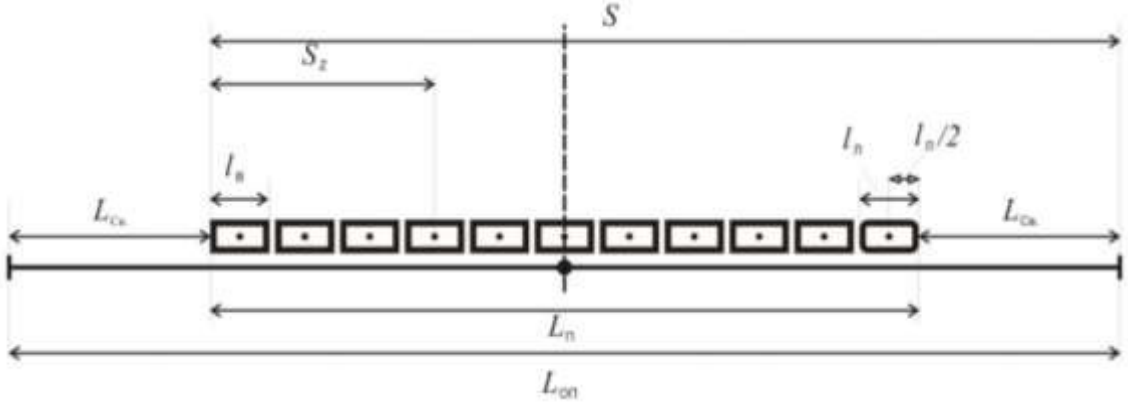

Fig.1 - Design scheme of the composition on the railway track

The value of the slope can be represented as a function of the path (Figure 2):

$$i(s) = \begin{cases} 0, & 0 < s < L_j \\ i_j, & L_j < s < L_{j+1} \end{cases}. \quad (4)$$

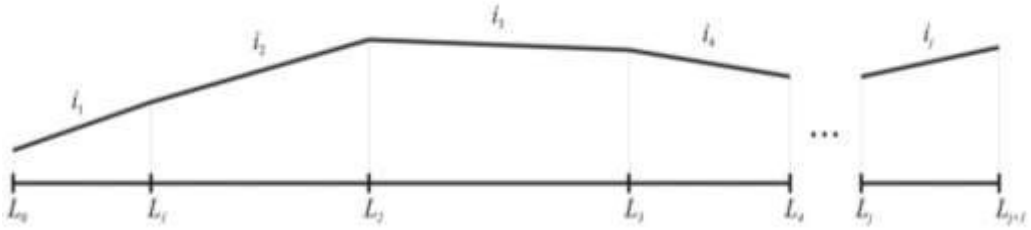

Fig.2 - Slope value (represented as a function of the path)

To determine the magnitude of the slope at which each material point is located, it is necessary to determine the dependence function on the path from the origin point, for which the middle PO of the departure station path is traditionally taken.

The path profile characteristic is usually set in tabular form by two parameters (Figure 2):

- projection of the length of the section on the horizontal L_j;
- the value of the corresponding slope i_j.

By modifying the table, that is, by writing the coordinates of the beginning and end of the section of the profile with the corresponding slope, we can obtain a function of the dependence of the slope on the coordinate of any point of the section:

$$i = \begin{cases} i_1, if\ 0 < S < L \\ i_2, if\ L_1 < S < L_2 \\ \dots\dots\dots\dots\dots\dots \\ i_n, if\ L_{n-1} < S < L_n \end{cases}. \quad (5)$$

The path of the locomotive from the origin is calculated as follows:

$$S_L = S_{\Pi_i} + \sum_{j=1}^{n/2} \cdot l_{B_j} + \frac{L_Л}{2}, \quad (6)$$

where l_{B_j} – is the length of the j-th car;

n – number of wagons;

$L_Л$ – length of the locomotive.

The path of the k-th wagon from the origin will be:

$$S_K^W = S_L - \sum_{j=1}^{n-K} \cdot l_{B_{Wj}}. \quad (7)$$

As a rule, traction calculation is carried out to transport the train from one railway station to the next along the stretch, having sections of different lengths with the corresponding slope.

The design scheme of the transporting with the boundary stations and the location of the train on it is shown in Figure 3.

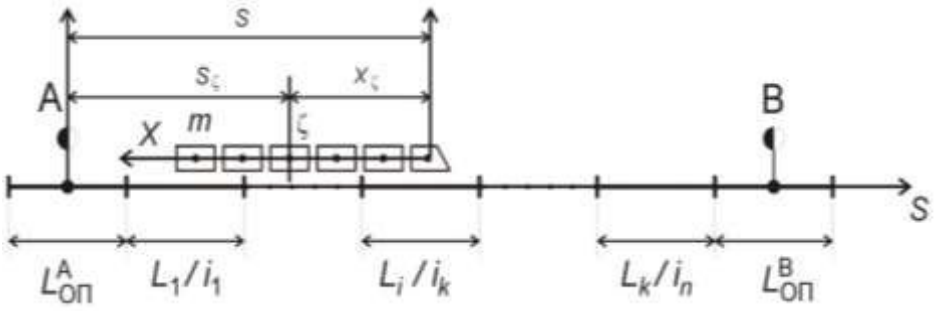

Fig.3 - Design scheme of the train during transportation

According to Figure 3, the point of the beginning of the movement is the middle of the receiving-sending tracks of station A, and the final point of the movement is the middle of the receiving-sending tracks of station B.

The slope characteristic can be described by the following relationship:

$$i = \begin{cases} 0, & \text{if } -\frac{L^A_{RC}}{2} < S < \frac{L^A_{RC}}{2} \\ & \dots\dots\dots\dots\dots\dots \\ i_k, & \text{if } \sum_{j=1}^{k-1} L_j + \frac{L^A_{RC}}{2} < S < \sum_{j=1}^{k} L_j + \frac{L^A_{RC}}{2} \\ & \dots\dots\dots\dots\dots\dots \\ 0, & if \ \sum_{j=1}^{n} L_j + \frac{L^A_{RC}}{2} < S < \sum_{j=1}^{n} L_j + \frac{L^A_{RC}}{2} + \frac{L^B_{RC}}{2} \end{cases}, \quad (8)$$

where S – is the current value of the coordinate of the center of mass of the locomotive;

k – is the number of the section with the corresponding slope;

n – is the last section of the stretch;

L_j – is the length of the section with the corresponding slope;

L^A_{RC} и L^B_{RC} – the length of receiving-sending tracks of the stations A and B.

Let us consider the following case of the location of the train: the center of mass of the locomotive is on section *k*, the train consists of *n* cars with the length l_w and one locomotive with the length l_L. If the center of mass of the locomotive is at S distance from the center of receiving-sending ways of the station of departure A, then the coordinate of the center of masses of the ζ-th wagon is determined for the mobile system of coordinates as:

$$X_\zeta = \frac{l_L}{2} - \sum_{j=1}^{\zeta} l_{w_j}, \quad (9)$$

where l_{w_j} – is the length of the j-th wagon;

l_L – length of the locomotive

The coordinate of the center of masses of the ζ-th wagon in the motionless system of coordinates:

$$S_\zeta = S - X_\zeta. \quad (10)$$

Based on the dependence (8), we determine the slope i_ζ on which the ζ-th wagon is located by the value S_ζ.

Thus, the total train resistance must be determined according to the following algorithm:

1) Having the current coordinate of the center of mass of the locomotive S, we determine the vector of paths of the center of mass of each wagon S_ζ by the formula (10).

2) Having characteristic matrix of the transportation represented by the length of the section and the corresponding slope, summing up the lengths of the sections and half the length of the receiving and sending paths of the departure station is performed. Summation is performed before the sum exceeds the path value S_ζ.

3) The number *k* of the last summed section is determined. The slope value for the ζ-th wagon is determined by the number of the previous section, that is «$k-1$», Thus, a vector is formed that determines the amount of slope on which each car is located.

4) The total resistance to movement is determined by the product of the mass of the wagon by the corresponding slope:

$$W^W_{sl} = \sum_{j=1}^{m} m_{W_j} \cdot i_j, \quad (11)$$

where m_{W_j} – mass of the j-th wagon;

i_j – slope of the section on which the j-th wagon is located;

m – number of cars in the train.

5) The resistance to locomotive movement is defined by the expression:

$$W_{Sl.}^{L} = m_L \cdot i_L \tag{12}$$

where m_L – mass of the j-th wagon;

i_L – slope of the section on which the locomotive is located, defined similarly to i_j.

3. Conclusion

The above methods make it possible to determine the resistance to the movement of the composition more accurately. Subsequently, it increases the convergence of the results of traction calculations with real indicators of the speed of movement and the path passed. However, it is necessary to determine the coordinates of the rail crews accurately and, first of all, the coordinates of the locomotive. On the main railway lines, it is solved using satellite navigation systems, in the subway by using floor (located on the rail tracks) sensors. In the field of industrial railway transport, both options listed are not fully suitable. The system with combined use of a small number of floor sensors together with locomotive speeds and a device for determining the actual slope of a track profile element [11] is considered to be perspective.

References

[1] Voronko V. A. Justification of the choice of parameters of shunting and industrial diesel locomotives taking into account operating conditions. Dissertation for the degree of candidate of technical sciences. / V. A. Voronko. – M.:, 2005. – 148 p.

[2] Shelest P. A. Modern industrial diesel locomotives. Scientific publication. / P.A. Shelest. – M.; Transport, 1978. – 224 p.

[3] Tyagovik // http://loko.su/level2/Program_0.html

[4] Muginshtein L. A. Energy-optimal traction calculation of train movement. / L.A. Muginshtein, A.E. Ilyutovich, I.A. Jabko // Vestnik of the Research Institute of Railway Transport. – 2013. – № 6. – p.3-13

[5] Nechai T. A. Models and algorithms of the specialized information-computer system for planning shunting work on industrial transport. Dissertation for the degree of candidate of technical sciences / T. A. Nechai. – Penza, 2019. – 150 p.

[6] Petrov U. P. Optimal vehicle traffic management. Scientific publication / U.P. Petrov. – L.: Energia, 1969. - 96 p.

[7] Pschyhopov V. H. Synthesis of energy efficient algorithms of electric train traffic control in conditions of overcoming heterogeneity of the track profile. / V.H. Pschyhopov, M.U. Medvedev, V.A. Shevchenko // Engineering newsletter of the Don – 2013. – № 4. – P. 88 – 94.

[8] Rozhkov A. V. Simulation of freight train movement to determine the energy-optimal modes of locomotive control in industrial enterprises conditions / A.V. Rozhkov, M.A. Nartov, T.R Bikenov // Actual problems of transport and energy: ways of their innovative solution: Proceedings of the VII International Scientific Conference. – L.N. Gumilyov Eurasian National University. – Astana, 2019. – P.163-168. – ISBN 978-601-80738-3-0.

[9] Rozhkov A. V. Freight train movement simulation for establishing energy-optimized locomotive handling modes for industrial facilities / A.V. Rozhkov, M.A. Nartov, T.R Bikenov // Vestnik KazATK. – 2019. – № 2. – P.76-82.

[10] Rozhkov A. B. Determination of specific resistance to train movement from the track slope at the specified traction calculation / A.B. Rozhkov, M.A. Nartov // Интеграция науки, образования и производства – основа реализации Плана нации Integration of science, education and production - the basis for the implementation of the Plan of Nation: матер. междунар. scientific conference, part 1. – Karaganda State Technical University. – Karaganda, 2019. – P.363-365. – ISBN 978-601-315-750-4.

[11] Rozhkov A. B. The device of control of safety of movement of an industrial locomotive on tracks with a large slope of a profile: the Patent of the Republic of Kazakhstan on useful model № 4885 / A.B. Rozhkov, O.T Balabaev, M.A. Nartov.

Mathematical model of plate movement in thixotropic mud

Kyzylbaeva E. Zh.[1], Kukesheva A.B.[1], Kunaev V.A.[2]
[1]Non-profit Joint-Stock Company Karaganda Technical University, Karaganda, Kazakhstan
[2]Karaganda Industrial University, Temirtau, Kazakhstan

Abstract. As the practice of construction production shows, intensification of construction by «the diaphragm wall method» promotes application of milling and drilling machines of mechanical and hydromechanical principles of action. However, their implementation is constrained by the lack of an appropriate scientific basis for calculating and constructing promising machines working in the drilling thixotropic mud. The authors conducted theoretical and experimental studies of the loading of the working organs of drilling and milling machines as they moved in the drilling mud. The first stage of the study produced formulas for determining friction forces for each of the possible modes of motion in a thixotropic mud of a smooth, small-thickness plate.

Keywords: The drilling thixotropic mud, the diaphragm wall method, the drilling machines, the milling machines, the small-thickness plate.

1. Introduction

During construction of buried structures using the diaphragm wall method, the excavation works, as usual, are performed under the drilling thixotropic mud [1]. The drilling mud fills the trench walls and is necessary to prevent their sides from collapsing during development (Fig.1).

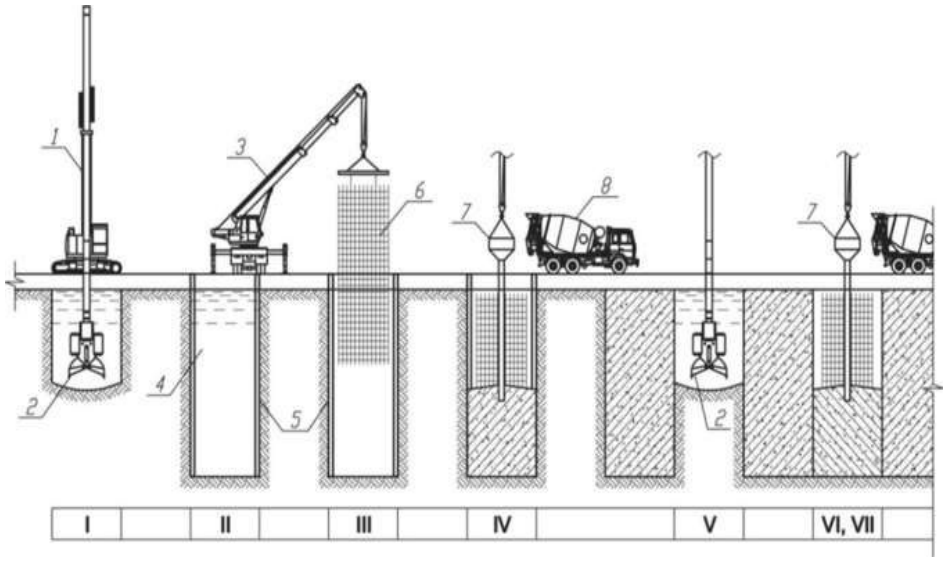

Fig.1 – Construction by «the diaphragm wall» method

There is a hypothesis that additional loading affects the working entity (WE) of a trench digger moving in the drilling mud. This makes it necessary to determine the amount and nature of the loading of the rotary working entity when it is moved in the drilling mud, to take into account the effect of the pressure of the mud on the bottom and its filtration rate in the ground by the value of the cutting force of the ground, determination of the nature of the variation of cutting forces according to the radius of the working entity and development of a method for the solid calculation of the structural elements of the working entity of milling and drilling machines[2,3]. According to the practice in construction production, the growth of construction by «the diaphragm wall method» makes it possible to use milling and drilling machines according to the principle of mechanical and hydromechanical action [4,5].

However, their introduction is made difficult by the lack of an appropriate scientific basis, which makes it possible to calculate and design promising machines working in the drilling thixotropic mud.

2. Results and discussion

The authors have carried out theoretical and experimental studies on the loading of the working organs of drilling and milling machines as they move in the drilling mud. The method for determining the resistance forces acting on the working entity from the side of the mud consists in presenting it as a set of flat bodies and rotating

bodies. At the first stage of the study, the motion in thixotropic mud of a smooth plate area and small thickness is considered (Fig. 2).

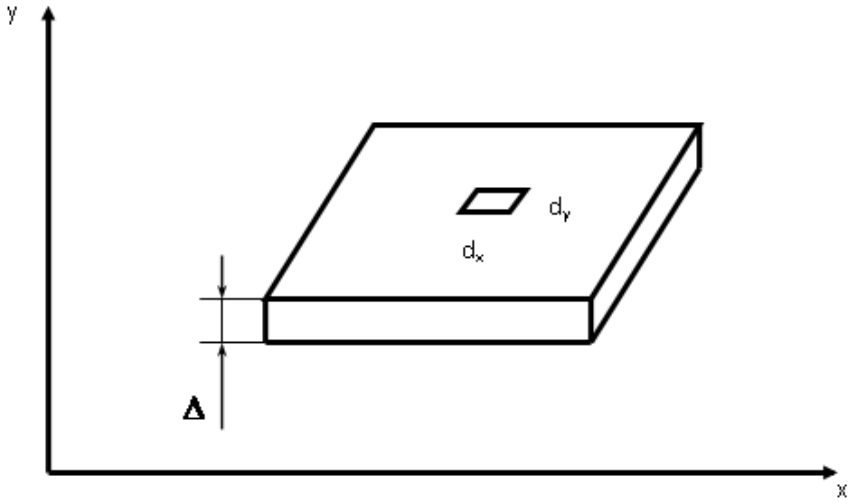

Fig.2 – The plate in the drilling mud

The motion of the plate in the drilling thixotropic mud, that may be forward, rotation and compound. If the velocity vector lies in the plate plane, the resistance to motion is determined by the friction force T arising on the side surfaces of the plate and the buoyancy force P_V. The hydrodynamic resistance due to the infinite small thickness of the plate can be neglected. The value of the total drag force R_c for various flow conditions of the mud will be different, this is due to a change in its rheology depending on the flow velocity. For the Swedish conditions, when the disc moves vertically, taking into account the Bingham-Kelvin model, it is true:

$$R_C = F\frac{\eta_1 \varepsilon E_1 E_2 + \sigma_0 t E_1 E_2}{\left[E_1(1-e^{\frac{t}{t_0}}) + E_2\right]\eta_1 + tE_1E_2} - m_n g, \tag{1}$$

where m_n – plate mass;

η – relaxational viscosity;

ε – relative strain;

E_1 – initial conditional instantaneous shear modulus;

E_2 – elasticity modulus;

σ_0 – elastic limit, below which the residual deformations cannot be developed;

t – time;

t_o - relaxation time.

When the plate moves in the horizontal direction and zero buoyancy:

$$R_C = F\frac{\eta_1 \varepsilon E_1 E_2 + \sigma_0 t E_1 E_2}{\left[E_1(1-e^{\frac{t}{t_0}}) + E_2\right]\eta_1 + tE_1E_2}. \tag{2}$$

The friction force with the plate motion at a speed causing appearance of the Bingham conditions of fluid flow can be determined by the following dependence:

$$T = F\tau = F\left(\tau_0 \pm \eta\frac{dU}{d\delta_t}\right), \tag{3}$$

where τ – shear stress;

τ_0 – yield stress.

The “plus” or “minus” sign is used depending on the velocity gradient sign taking into account the requirement to make positive the specific force direction τ [6].

In the straight line motion of the plate in the drilling mud, its speed is equal to the speed of the flow core, which follows from the added masses theory. Considering the $\Delta\rho = 0$, what corresponds to our case, we have:

$$U = -\frac{\tau_0}{\eta}\left(H_{\max} - \delta_T\right), \tag{4}$$

where U – fluid motion speed;

H_{maz} – maximum distance from the plate;

δ_T – boundary-layer thickness;

η – plastic viscosity.

Then the plate velocity gradient in the following:

$$\frac{dU}{d\delta_T} = \frac{\tau_0}{\eta}. \tag{5}$$

The friction force under the condition $V_n = U_{\max}$ can be determined by the following formula:

$$T = F\tau = F\left(\tau_0 + \eta\frac{dV_n}{dn}\right) = 2F\tau_0. \tag{6}$$

In the pseudo-laminar conditions of motion the rheological properties of the drilling mud are adequate to the rheological properties of an ordinary viscous fluid. The velocity-distribution law of viscous fluid flow has a parabolic nature:

$$U = U_{\max}\left(1 - \left(\frac{\delta_T}{H_{\max}}\right)^2\right). \tag{7}$$

The plate velocity gradient:

$$\frac{dU}{dn} = -2U_{\max}\frac{\delta_T}{H_{\max}}. \tag{8}$$

The plate friction force in the mud can be determined by the following formula:

$$T = F\tau = \pm 2F\mu_p\frac{dU}{dn} = \pm 2F\mu_p U_{\max}\frac{\delta_T}{H_{\max}}, \tag{9}$$

where μ_p - dynamic viscosity.

The maximum value of the friction force corresponds to the equality of the values $H_{\max}$ and δ_T, in this case:

$$T_{\max} = \pm 2F\mu_p\frac{U}{H_{ж}}. \tag{10}$$

Assuming the motion speed for the mud flow to be equal to the speed of the plate motion, we obtain:

$$T_{\max} = \mp 2F\mu_p\frac{V_n}{H_{ж}}. \tag{11}$$

In the stream core of turbulent flow with the developed turbulence speed the fluid flow changes according to the logarithmic law:

$$U = \left(U^* \ln\delta_T\right)/\left(\beta + c\right), \tag{12}$$

where U^* – dynamic velocity or fluid cutting speed;

β – constant L. Prandtl, β =0,360…0,436

C – constant value.

The plate velocity gradient:

$$\frac{dU}{d\delta_T} = \frac{U^*}{\beta\delta_T}. \tag{13}$$

Then, taking into account the shear function during turbulent motion of the mud [7], we have:

$$\tau = \mu_\phi \frac{dU}{d\delta_T} + \rho_C l^2 \left(\frac{dU}{d\delta_T}\right)^2 = U^* \left[\frac{\mu_\phi}{l} + \rho_C l \left(U^*\right)^2\right], \tag{14}$$

μ_ϕ – fictitious velocity.

$$T = F\tau = F\frac{U^*}{l}\left(\mu_\phi + \rho_C l U^*\right). \tag{15}$$

Moreover, as it appears from the theory of turbulent motion that $l = \beta\delta_m$.

When the plate rotates around a horizontal or vertical axis, the moment M_c from the resistance force to motion is determined in the general case by the following dependence:

$$M_C = \left[P_{zo} + T + (P_V - mg)\sin\varphi\right]R,$$

where φ – plate rotation angle about axis of rotation.

P_{zo} – hydrodynamic resistance.

In case of the plate complex motion, when determining its speed, it is necessary to take into account the value of the angle α between the portable V and relative ωR speeds:

$$\alpha = arctg\frac{V}{\omega R}.$$

For excavating machines (drilling and milling), as a rule, the portable speed is one or two orders of magnitude less than the relative, and the value of the α angle does not exceed 2...3°.

3. Conclusions

Thus, there have been obtained the formulas for determining the friction forces for each possible motion conditions of the drilling thixotropic mud. The following conclusions have been made:

1. During the Swedish conditions of the drilling mud motion the resistance to the plate motion is provided by occurring of elastic strains.

2. The plate loading under the Bingham conditions of the mud flow is characterized by its ultimate shear stress τ_0 .

3.The resistance to plate motion during the pseudo-laminar motion of the mud depends on the mud viscosity and its speed.

4. In the turbulent conditions of motion, the resistance force to the plate motion depends on the core size of the flow stream, the medium density, and the fictitious viscosity value.

5. Supplementing the results with data on the loading of the bodies of rotation will make it possible to establish the resistance acting on the working entity of the earth-moving machine.

References

[1] Smorodinov M.I., Fedorov B.S. Installation of structures and foundations by the «the diaphragm wall method» - M.: Stroyizdat, 1986. – 216 p.

[2] Kadyrov A.S., Kabashev R.A. Basic loading of milling and drilling machines. – Karaganda, KSTU, 1999. – 124p.

[3] Ogibalov P.M., Mirzajanzade A.H. Non-stationary movement of viscoplastic media. - M.: MSU, 1970. – 415 p.

[4] Kochetkova R.G. Influence of modern stabilizers on improved properties of clayey soils // Journal of “Soil Mechanics and Foundation Engineering”, Vol. 49, Issue 1, 2012–p. 12-15.

[5] Aliev S.B., Suleev B.D. Study and calculation of the disk-millingt // “Ugol” – Russian Coal Journal, 2018, № 11/ - P.32-34.

[6] Zhunusbekova Zh. Zh., Kadyrov A. S. Study of digging machine flat element loading in clay solution // Scientific Bulletin of National Mining University Scientific and technical journal, Dnipropetrovsk, State Higher Educational Institution “National Mining University”, 2016, no 2 (152). – P.. 30-34.

[7] Kadyrov A.S., Amangeldiev N.E. New specifications of the theory of ground cutting. Periódico tchê química, 2019, Vol. 16 N. 31.